Running title: miR-200-3p suppresses nephroblastoma cells

microRNA-200c-3p suppresses proliferation and invasion of nephroblastoma cells by targeting EP300 and inactivating the AKT/FOXO1/p27 pathway

Juan Cao[1,2,3], Guang-Shu Liu[4], Ning-Zhen Zou[5], Huang Zhang[2], Xiao-Xiao He[2], Ping-Li Sun[1,3], Hong-Jian An[1,3], Hong Shen[1,3,*]

[1]Department of Pathology, Southern Medical University, Guangzhou, Guangdong, China; [2]Department of Pathology, Shenzhen Children's Hospital, Shenzhen, Guangdong, China; [3]Guangdong Province Key Laboratory of Molecular Tumor Pathology, Guangzhou, Guangdong, China; [4]Department of Pathology, The Eighth Affiliated Hospital, Sun Yat-sen University, Shenzhen, Guangdong, China; [5]Department of Pathology, Guangdong Medical University, Zhanjiang, Guangdong, China

*Correspondence: shenhong2010168@163.com

miR-200c-3p is aberrantly expressed in numerous cancers, but its underlying mechanisms in nephroblastoma are unknown. In our study, the differentially regulated miRNAs between the nephroblastoma tissues and adjacent non-neoplastic renal tissues were screened based on microarray analysis. The miR-200c-3p expression in nephroblastoma tissues and cells was detected by qRT-PCR. Then, the effects of miR-200c-3p mimic or inhibitor on cell proliferation, invasion, and migration were evaluated by CCK-8 assay, plate colony formation assay, soft agar assay, Transwell, and wound-healing assay in SK-NEP-1 and G401 cells. Afterward, the target gene of miR-200c-3p was predicted by TarBase, miRTarBase, miRDB softwares, and then verified by dual-luciferase reporter gene assay. The in vivo effects of miR-200c-3p on pathological changes and tumor volume were investigated in tumor xenograft mice by H&E staining and in vivo fluorescence imaging. ChIP assay was used to evaluate the relationship between histone acetyltransferase E1A-binding protein p300 (EP300) and P27, and the relationship of the role of miR-200c-3p in nephroblastoma and the AKT/FOXO1/p27 signaling pathways was evaluated by western blotting. Our study shows that miR-200c-3p was downregulated in nephroblastoma tissues and cells, and EP300 was a target gene of miR-200c-3p. Furthermore, miR-200c-3p mimic decreased cell proliferation and inhibited cell migration and invasion in nephroblastoma. Mechanistically, miR-200c-3p could inhibit p-AKT activity and enhance p-FOXO1 and p27 expression. Notably, the transcription factor P27 could bind to the EP300 promoter. This study demonstrates a new approach to treat nephroblastoma.

Key words: miR-200c-3p; nephroblastoma; EP300; AKT/FOXO1 pathway; proliferation; invasion

46 Nephroblastoma is an embryonal kidney neoplasia and is found in children younger than five years

47 old. Unfortunately, the relapse rate of nephroblastoma is up to 15% [1-3]. Therefore, to investigate

48 the mechanism of nephroblastoma development and pathogenesis is very important. These reports

49 showed aberration expression of WT1, abnormalities of 11p15 methylation, and Wnt-activating

50 mutations in nephroblastoma were usually common. In recent years, the comprehensive genomic

51 analyses of nephroblastoma identified novel mutations in DROSHA, DGCR8, and DICER1 genes

52 due to the aberrantly regulation of miRNA [4-6]. Despite these efforts, recurrent driver mutations

53 were not identified in most nephroblastomas [7].

54 microRNAs (miRNAs), is transcribed by RNA polymerase II to produce small noncoding RNA(19-

55 25 nt) [8, 9]. These reports showed that miRNAs can bind to the complementary sequences of the

56 3'-untranslated region (3'-UTR) in their target mRNAs to inhibit about 20-30% gene mRNA

57 transcription and protein translation [10, 11]. In multiple cancers, miRNAs can bind 3'-UTR of

58 oncogenes or tumor-suppressor genes to downregulate the gene expression and participate in the

59 cancer metastasis [12]. Although miRNAs plaied key roles in cancer progression, the detailed

60 molecular regulatory mechanisms of miRNAs in cancer were not well understood. In the our

61 research, we investigated the expression of miR-200c-3p in nephroblastoma and further explored its

62 target gene and molecular mechanisms, which might provide novel targets for the treatment of

63 nephroblastoma.

64 In this study, our study showed that miR-200c-3p was downregulated in nephroblastoma tissues and

65 cells, which played a key role in the progression of nephroblastoma. Moreover, we found that miR-

66 200c-3p inhibited the proliferation and invasion of nephroblastoma by targeting EP300 and

67 inactivating AKT/FOXO1/p27 pathway. The molecular mechanisms might provide new insights

68 and therapeutic strategies for nephroblastoma prevention and treatment.

69

70 **Patients and methods**

71 **Cell lines and human tissue samples.** Human nephroblastoma cell lines SK-NEP-1, G401 and

72 human embryonal kidney cells 293FT cells were obtained from Shanghai Cell Bank of Type

73 Culture Collection (Shanghai, China). SK-NEP-1 cells were cultured in McCoy's 5A medium

74 (HyClone, Logan, Utah, USA) and G401 cells were cultured in RPMI-1640 medium (HyClone,

75 Logan, Utah, USA). All cell lines supplemented with 10% fetal bovine serum (HyClone, Logan,

Utah, USA) at 37 °C under 5% CO_2. Fresh nephroblastoma tissues and adjacent non-neoplastic renal tissues were collected from 22 patients who underwent nephroblastoma resection without prior radiotherapy and chemotherapy at the Department of Urology Surgery in Shenzhen Children's Hospital (Shenzhen, Guangdong Province, People's Republic of China) in 2018. These samples were collected immediately after resection, snap-frozen in liquid nitrogen, and stored at -80 °C until needed.

The study protocol was performed in accordance with the guidelines outlined in the Declaration of Helsinki. For the clinical patient tissues used in this study, prior patient consent and approval from the Institutional Research Ethics Committee (IREC) were obtained.

Microarray analysis. The miRNA expression patterns among adjacent non-neoplastic renal tissues (Normal) and nephroblastoma tissues without lymphatic metastasis were analyzed using human miRNA Paraflo™array (CapitalBio Technology laboratory, Beijing, China). Three clinical samples were pooled in each group.

Construction of plasmids and transfection. Lentiviral constructs expressing miR-200c-3p (Lenti-miR microRNA precursor clone collection; System Biosciences, Carlsbad, CA, USA) were packaged using the pLP1/pLP2/pLP VSV-G lentivector Packaging Kit (Invitrogen, Foster city, CA, USA). Lentiviral constructs were used to infect nephroblastoma cell lines to establish cells stably expressing miR-200c-3p. miR-200c-3p inhibitor and its negative control antisense oligos, were obtained from Genechem Company (Shanghai, China), and were used to transfect indicated cells, according to the manufacturer.

Cell proliferation assay. For analysis of the impacts of miR-200c-3p on cell proliferation in nephroblastoma, 1×10^3 SK-NEP-1 and G401 cells were respectively seeded into 96-well plates, and then transfected with miR-200c-3p mimic, mimic NC, miR-200c-3p inhibitor or NC inhibitor using the Lipofectamine™ 3000 transfection reagent (Thermo Fisher Scientific, USA). At each time point,10 μl CCK-8 assay reagent (Beyotime, China) was added into each well of the 96-well plates. The absorbance density at a wavelength of 450 nm was measured after 2 h of incubation at 37 °C. Each cell group was plated in three duplicate wells. All experiments were performed three times.

Plate colony formation assay. Totally, 1×10^2 G401 cells were added to each well of 6-well culture plates, and then transfected with miR-200c-3p mimic, mimic NC, miR-200c-3p inhibitor or NC inhibitor using the Lipofectamine™ 3000 transfection reagent (Thermo Fisher Scientific, USA).

3

The cells were incubated at 37 °C for 14 days. Then the colonies were washed twice with phosphate-buffered saline，fixed with 4% paraformaldehyde for 5 min and stained with Giemsa solution. The number of colonies containing 50 cells or more was counted under a microscope [plate clone formation efficiency=(number of colonies/number of cells inoculated)] × 100%).

Cell cycle assay. Briefly, the SK-NEP-1 and G401 cells that transfected with miR-200c-3p mimic, mimic NC, miR-200c-3p inhibitor or NC inhibitor were harvested by trypsin and fixed by 70% ethanol. Following cell centrifugation, the cells were stained with 10 μg/ml of propidium iodide (PI) for 30 min at room temperature. Lastly, the cell cycle of the treated cells were observed and analyzed using a FACScan flow cytometer (BD Biosciences , USA) thereafter. The proliferative index was calculated as (S+G2/M)/(G0/G1+S+G2/M) × 100%.

Transwell matrigel invasion assay. Briefly, 8 μm Boyden invasion chambers were rehydrated with RPMI 1640 (serum-free) for 2 h at 37 °C. Next, 1.5×10^5 G401 cells in serum-free RPMI 1640 were seeded to the upper compartment of the chamber cells, and treated with miR-200c-3p mimic, mimic NC, miR-200c-3p inhibitor or NC inhibitor. Then RPMI 1640 culture medium containing 20% fetal bovine serum was added to the lower compartment as the chemotactic factor and the chambers were incubated at 37 °C for 24 h. The noninvasive cells were removed with a cotton swab. Cells that migrated through the membrane and stuck to the lower surface of the membrane were stained with hematoxylin and counted under a light microscope (Olympus, Japan) in 5 random visual fields (200×). Each experiment was repeated 3 times.

Wound healing assay. G401 cells were inoculated in 6-well plates. After growing to 95% of confluence, cells were wounded by scratching the vertical lineation using pipette tips, followed by culturing in RPMI 1640 without serum. It was suggested to perform the wound healing assay under without serum and under 10% serum to confirm that the observed effect was caused by the cell migration and proliferation or by cell migration only. Subsequently, cells were treated with miR-200c-3p mimic, mimic NC, miR-200c-3p inhibitor or NC inhibitor, respectively. The distance of the scratch and migrated rate were observed at 0, 24, 48 and 72 h using a light microscope (Olympus, Japan).

Tumor xenograft. Four-week-old athymic BALB/c nu/nu mice were purchased from the Central Laboratory of Animal Science at Southern Medical University (Guangzhou, China). The mice were housed in our laboratory in a specific pathogen-free environment. To establish the tumor xenograft

4

mice, 1×10^7 SK-NEP-1 cells were injected subcutaneously into right flank of nude mice. Mice (n=4, each group) were exposed with saline (Blank group), Mimic NC (Mock group), miR-200c-3p mimic, and miR-200c-3p inhibitor via intraperitoneal injection. Tumor lengths (L) and widths (W) were measured from day 5 to day 28 using a digital caliper, and tumor volumes were calculated using the equation volume (mm^3)=L × W^2/2. Meanwhile, *in vivo* fluorescence imaging on the IVIS Platform (720p) (PerkinElmer , USA) was performed at 14 and 28 days after transplantation. All animal experiments were conducted in strict accordance with the principles and procedures approved by the Committee on the Ethics of Animal experiments of Southern Medical University, China.

Histological evaluations. The histological alterations in the tumor tissues were evaluated by the Haematoxylin and Eosin (H&E) (PH0516, Phygene, China) staining. Briefly, tumor tissues were fixed with 4% paraformaldehyde and embedded in routine paraffin. After being dewaxed and hydrated, the renal tissue slides were subjected to H&E staining following standard procedures. Lastly, the sections were observed under a light microscope (Olympus, Japan).

Quantitative real-time PCR (qRT-PCR). Total RNA, including miRNA from the tissue samples and cultured cells was extracted using Trizol reagent (Invitrogen, USA) according to the manufacturer's instructions. The level of miR-200c-3p was analyzed by qRT-PCR using All-in-One miRNA qRT-PCR Detection Kit (GeneCopeia, USA). cDNA was synthesized from total RNA using TaKaRa reverse transcription kit (TaKaRa, China) , and real-time PCR was performed for the detection of miR-200c-3p and EP300. The miR-200c-3p specific forward primer: 5'-GGATAATACTGCCGGGT -3' ; specific reverse primer: 5'-GTGCGTGTCGTGGAGTC-3', and the fragment length was 214bp; U6 was amplified as an internal control. The U6 specific forward primer: 5'-GCTTCGGCAGCACATATACTAAAAT-3'; specific reverse primer: 5'-CGCTTCACG AATTTGCGTGTCAT-3' (also used as the reverse primer), and the fragment length was 163bp. The relative expression was calculated using the $2^{-\Delta\Delta Ct}$ method. All experiments were performed in triplicate.

Luciferase activity assay. The polymerase chain reaction (PCR) was profermed to amplify the 3'UTR region of the EP300 gene which the miR-200c-3p binding and then the product of PCR was inserted into the vector. A mutant construct in two miR-200c-3p binding sites of EP300 3'UTR region also was generated using Quick Change Site-Directed Mutagenesis Kit (Agilent Technologies, USA). Co-transfections of EP300 3'UTR or mutEP300 3'UTR plasmid with miR-200c-3p lentivirus vector into the cells were accomplished using Lipofectamine™ 3000 (Thermo

168 Fisher Scientific, USA). Luciferase activity was measured using the Dual-Luciferase Reporter

169 Assay System (Promega, USA) after 48 h transfection. Each assay was repeated in 3 independent

170 experiments.

171 **Western blotting analysis.** The RIPA buffer (1× phosphate-buffered saline, 1% NP40, 0.1%

172 sodium dodecyl sulfate, 5mmol/l EDTA, 0.5% sodium deoxycholate, and 1 mmol/l sodium

173 orthovanadate) and protease inhibitors were used to extract protein from cells, and quantified by

174 BCA protein assay kit (#P0012, Beyotime, China). 50 μg protein lysates were resolved on 10%

175 sodium dodecyl sulfate-polyacrylamide by gel electrophoresis and electro transferred to

176 polyvinylidene fluoride (PVDF) membranes (Immobilon P, Millipore, USA). The membranes were

177 blocked with 5% non-fat milk solution for 1 h, and incubated with anti-EP300 antibody (1:1,000,

178 cat. no.70088, CST, USA), anti-Akt antibody (1:1,000, cat. no.4691, CST, USA), anti-p-Akt

179 antibody (1:2,000, cat. no.4060, CST, USA), anti-FOXO1 antibody (1:1,000, cat. no.2880, CST,

180 USA), anti-p-FOXO1 antibody (1:1,000, cat. no.84192, CST, USA) and p27 antibody (1:1,000, cat.

181 no.3688, CST, USA) overnight at 4°C. After Tris Buffered Saline Tween (TBST) washing, the

182 membranes were followed by horseradish-peroxidase-conjugated secondary antibodies (cat.

183 no.5571, CST, USA) and the signal was detected using an enhanced chemiluminescence reaction

184 performed according to the manufacturer's instructions (Alpha Innotech, CA, USA). Image density

185 of immunoblotting was determined by gel densitometry (Bio-Rad, PA, USA). The experiments

186 were independently repeated in triplicates.

187 **Chromatin immunoprecipitation (ChIP) assay.** To further investigate the mechanism of miR-

188 200c-3p involved in the cell proliferation and migration of nephroblastoma, ChIP assay was used to

189 evaluate the relationship between EP300 and P27. Briefly, cells were collected and treated with 1%

190 formaldehyde to performe the cross-linking of protein and chromatin. Then, 0.125 M glycine

191 terminated the cross-linking on ice. After cell disruption by ultrasonic oscillation, the chromatin

192 DNA with the short fragments was extracted and reacted with EP300 antibody(cat. no.12281, CST,

193 USA; IP group) or IgG (cat. no.2729, CST, USA; negative control), followed by incubation with

194 protein A/G beads, and decrosslinking with proteinase K. Lastly, DNA were extracted to perform

195 qRT-PCR based on the primers that were designed according to the 3 binding site between EP300

196 promoter and P27 (Table 1).

197 **Statistical analysis.** All statistical analyses were performed using SPSS 20.0 statistical software

198 and were calculated from 3 independent experiments. Differences between sample groups and

6

199 within each sample group were analyzed by one-way ANOVA or by independent-samples t test.

200 Quantitative values are expressed as the mean±SD and p-value of < 0.05 was considered

201 statistically significant in all experiment.

202

203 **Results**

204 **Downregulation of miR-200c-3p in nephroblastoma tissues and cells.** To identify the miRNAs

205 that regulate the proliferation and invasion in nephroblastoma, we performed miRNAs array on

206 nephroblastoma tissues and adjacent non-neoplastic renal tissues (n=3/group). The Figure 1A

207 showed the differentially regulated miRNAs between the nephroblastoma tissues and adjacent non-

208 neoplastic renal tissues. From the list of differentially expressed miRNAs (Supplementary Table

209 S1), we found that miR-200c-3p was one of the most significantly downregulated miRNAs in

210 nephroblastoma tissues. However, the underlying mechanism by which the miR-200c-3p in

211 proliferation and invasion in nephroblastoma remain unclear. Firstly, we performed real-time PCR

212 analyses to test miR-200c-3p expression levels in 22 paired fresh nephroblastoma tissues and

213 adjacent non-neoplastic renal tissues. Results showed that miR-200c-3p level in the nephroblastoma

214 tissues was significantly lower than that in the adjacent non-neoplastic renal tissues ($p < 0.01$,

215 Figures 1B, 1C). Moreover, real-time PCR analyses were also used to explore the miR-200c-3p

216 expression levels in nephroblastoma cells (G401 and SK-NEP-1 cells) and human embryonic

217 kidney cells (293FT cells). We found that miR-200c-3p expression in G401 cells and SK-NEP-1

218 cells was significantly lower than that in 293FT cells ($p < 0.05$, Figure 1D). These results indicated

219 that miR-200c-3p was downregulated in nephroblastoma, and might be participated in

220 nephroblastoma proliferation and invasion.

221 **EP300 is a direct target of miR-200c-3p in nephroblastoma.** To identify target genes of miR-

222 200c-3p, we used three mRNA target-predicting algorithms, including

223 TarBase(http://carolina.imis.athena-innovation.gr),miRTarBase (http://mirtarbase.mbc. nctu.edu.tw),

224 miRDB (http://www.mirdb.org/) and based on the presence of binding sites in the 3'UTR region.

225 We found that the mRNA levels of 9 candidate target genes, including *AKT2*, *CRKL*, *CBL*, *EP300*,

226 *LAMC1*, *PTEN*, *E2F3*, *CCNE2*, and *CDK2*, were obviously up-regulated in G401 cells and SK-

227 NEP-1 cells compared with 293T cells ($p < 0.05$, Table 2). Then the miR-200c-3p mimic

228 experiments showed that compared with G401 cells transfected with mimic NC, the mRNA levels

229   of 5 candidate target genes, including *AKT2*, *CRKL*, *CBL*, *EP300*, and *CCNE2*, were remarkably

230   down-regulated in cells transfected with miR-200c-3p mimic ($p < 0.001$, Table 3). To explore the

231   direct relationship between miR-200c-3p and these 5 candidate target genes, we cloned the wide

232   type (WT) 3'UTR or mutation (Mut) 3'UTR of these 5 genes into a dual-luciferase UTR vector.

233   Notably, miR-200c-3p repressed 3'UTR of EP300 and CCNE2 in G401 cells, but had no effect on

234   the activity of Mut EP300 3'UTR ($p < 0.05$, Figures 2A, 2B) and Mut CCNE2 3'UTR

235   (Supplementary Figure S1A). However, dual-luciferase assay showed that miR-200c-3p could not

236   bind to 3'UTR of AKT2, CRKL, and CBL (Supplementary Figure S1A). Furthermore, with miR-

237   200c-3p inhibitor treatment in SK-NEP-1 and G401 cells, we found that the protein levels of

238   endogenous EP300 and CCNE2 were increased. In contrast, ectopic expression of miR-200c-3p

239   significantly reduced the protein levels of endogenous EP300 and CCNE2 in SK-NEP-1 and G401

240   cells ($p < 0.05$, Figure 2C, Supplementary Figure S1B). Notably, EP300 can enter the nucleus and

241   bind to enhancers or promoters, thereby greatly facilitating transcription initiation and activation

242   [13]. Thus, in this study, EP300 was selected as the target gene of miR-200c-3p for the following

243   experiments.

244   **miR-200c-3p inhibits proliferation of nephroblastoma cells.** To further investigate the biological

245   effect of miR-200c-3p in nephroblastoma cells, SK-NEP-1 and G401 cells were treated with miR-

246   200c-3p mimic or inhibitor. CCK8 assay showed that miR-200c-3p mimic significantly inhibited

247   the growth rate of SK-NEP-1 and G401 cells compared with blank group (Figure 3A). Colony

248   formation assay showed that overexpression of miR-200c-3p decreased the colony number of G401

249   cells (Figure 3B). Since SK-NEP-1 cells are semi suspended cells, colony formation assay was not

250   performed. Similarly, soft agar assay also revealed decreased colony number both in SK-NEP-1 and

251   G401 cells after miR-200c-3p mimic treatment (Figure 4A). Conversely, miR-200c-3p inhibitor

252   yielded the opposite effect on cell proliferation of nephroblastoma cells (Figures 3A, 3B, 4A). In

253   addition, cell cycle assay also found that the miR-200c-3p mimic caused a significantly decreased S

254   phase cell population, and a increased cell population in G0/G1 phase in SK-NEP-1 and G401 cells

255   (Figure 4B). indicating that the miR-200c-3p mimic could elicit G0/G1 phase cell cycle arrest.

256   Conversely, miR-200c-3p inhibitor yielded the opposite effect on cell proliferation of

257   nephroblastoma cells (Figures 3A, 3B. 4A, 4B).

258   **miR-200c-3p inhibits invasion and migration of nephroblastoma cells.** To investigate the role of

miR-200c-3p played in invasion and migration of nephroblastoma cells, we performed transwell invasion assay on miR-200c-3p tranducted nephroblastoma cells. The result showed that miR-200c-3p mimic significantly decreased the number of invading cells; conversely, miR-200c-3p inhibitor obviously increased the number of invading cells (Figure 5A). Wound healing assay was employed to examine the cells migration, and the result showed that miR-200c-3p mimic suppressed migration of nephroblastoma cells compared to the control cells (Figure 5B).When miR-200c-3p inhibitor treated the G401 cells, miR-200c-3p suppressed migration could be reversed (Figure 5B). Since SK-NEP-1 cells are semi suspended cells, Wound healing assay was not performed. Our results demonstrated that miR-200c-3p can inhibits invasion and migration of nephroblastoma cells.

miR-200c-3p inhibits tumor cell proliferation of nephroblastoma *in vivo*. Moreover, we also explored the effect of miR-200c-3p on cell proliferation *in vivo*. H&E staining of tumor tissues showed that the tumor cells in the miR-200c-3p mimic group was less than that in the other groups, and necrotic tissue was seldom observed in the tumor tissue, accompanied by inflammatory cell reaction, reduced nuclear division and cell atypia. However, in the Blank group, Mock group and miR-200c-3p inhibitor group, tumor cell proliferation was obvious, but inflammatory response was not obvious (Figure 6A). The subcutaneous tumor volume in the miR-200c-3p mimic group was significantly decreased compared to the blank or mock group. And when using miR-200c-3p inhibitor treatment, the tumor volume was drastically increased (Figure 6B). Moreover, in vivo fluorescence imaging revealed that tumor formation was not obvious in nude mice of miR-200c-3p mimic group at 14 days compared with the Mock group. However, all nude mice in the Mock and miR-200c-3p inhibitor groups showed significant subcutaneous neoplasms 14 days after transplantation (Figure 6C). On 28 days after transplantation, tumor was formated in nude mice of miR-200c-3p mimic group, and all nude mice in the Mock and miR-200c-3p inhibitor groups showed enlarged subcutaneous neoplasms compared that at 14 days (Figure 6C). Thereby our results revealed that miR-200c-3p inhibited the tumor growth of nephroblastoma.

miR-200c-3p is involved in AKT/FOXO1/p27 signaling pathways in nephroblastoma cells. Numerous studies have shown that miR-200c-3p suppressed proliferation and invasion by inactivating the AKT pathway in some human carcinomas [14, 15]. In our study, we analysed whether miR-200c-3p participates in the proliferation and invasion of nephroblastoma by activating or inhibiting AKT/FOXO1 pathway. The upregulation of miR-200c-3p markedly suppressed the

9

289 phosphorylation of AKT, and enhanced phosphorylation of FOXO1 and p27 expression compared

290 to both the blank and mock groups (Figure 7A). Conversely, inhibiting miR-200c-3p demonstrated

291 a reverse effect. No changes in the total protein levels of AKT and FOXO1 were observed under

292 any these conditions (Figure 7A). To detect whether p27 bind to EP300 promoter, we performed

293 ChIP assay immunoprecited with anti-p27 antibody. The result revealed that the positive bands

294 based on the 3 binging sites were successfully amplified by qRT-PCR in the IP group but not in the

295 IgG group (Figure 7B), which suggested that the transcription factor cound bind into the EP300

296 promoter. These results indicated that miR-200c-3p regulate the AKT/FOXO1 pathway via EP300

297 to play a role in nephroblastoma.

298

299 **Discussion**

300 According to gene expression regulation reports, it is widely recognized that miRNAs can decrease

301 gene expression by binding the 3'-UTR of their target genes and participate into many key

302 biological processes of cancer progression, such as tumor initiation, cell proliferation and metastasis

303 [16]. MiR-200c is the predominant member of the miR-200 family, which suppresses epithelial-

304 mesenchymal transition , invasion and metastasis in multiple cancers [17, 18]. The significance of

305 miR-200c-3p in cancer biology is more and more important. Such as miR-200 family members

306 were shown to negatively regulate tumour metabolism and progression by targeting lactate

307 dehydrogenase A. MiR-200c-3p played a tumor suppressive role through inhibited High mobility

308 group box 3 (HMGB3) in glioblastoma multiforme [19]. Another study showed that miR-200c-3p

309 tumor suppressor function might contrast with the induction of PD-L1, β-catenin and c-Myc

310 expression by paclitaxel/carboplatin, olaparib and radiation treatments in epithelial ovarian cancer

311 [20]. Evidence had shown that upregulated miR-200c-3p inhibited expression of SOX2, thereby

312 inhibiting development of renal cell carcinoma cells via modulating the Wnt/β-catenin signaling

313 pathway activation [21]. However, the data about the role of miR-200c-3p in nephroblastoma was

314 rarely published. Therefore, we examined its mechanism of action in the proliferation and invasion

315 of nephroblastoma cells.

316 Histone acetyltransferase E1A-binding protein p300 (EP300) is a ubiquitously expressed pleiotropic

317 multidomain coactivator that catalyzes acetylation of histone and nonhistone proteins [22]. EP300

318 mutations contribute to an unfavorable phenotype in a number of solid tumors and hematological

malignancies and therefore EP300 is often considered as tumor promoter [23]. Pathological studies have shown that EP300 was highly expressed in many tumors. For example, large breast cancer gene expression data sets revealed that EP300 expression was positively correlated with the expression of cancer stem cells markers and poor prognosis in triple negative breast cancer and basal-like breast cancer [24]. As a mechanism of action, EP300 mutations activated the NOTCH signaling pathway by negatively regulating a key FBXW7(NOTCH repressor), resulting in tumor progression in diffuse large B-cell lymphoma [25]. Esophageal squamous cell carcinoma clinical analyses showed that EP300 promotes epithelial-to-mesenchymal transition process, angiogenesis and hypoxia, and high expression and mutation of EP300 correlates with poor prognosis, thus it may act as an oncogene [26]. EP300, as a transcriptional coactivator, can participate in the regulation of a wide range of biological processes such as proliferation, cell cycle regulation, cell apoptosis and cancer differentiation [27, 28]. Thus, the overexpression of EP300 might contribute to the progression of multiple cancers [29]. However, the mechanism of EP300 in the proliferation and invasion of nephroblastoma is rarely known.

Our research investigated the miR-200c-3p-mediated mechanism in nephroblastoma. The expression of miR-200c-3p was significantly lower in nephroblastoma tissues than the adjacent non-neoplastic renal tissues by miRNAs array. Similarly, the expression of miR-200c-3p were lower in G401 and SK-NEP-1 cells than 293FT cells by real-time PCR. The CCK-8 assay, colony formation assay, soft agar assay and cell cycle assay were used to detect proliferation of nephroblastoma cells. We performed transwell invasion assay and wound healing assay to prove invasion and migration of nephroblastoma cells *in vitro*. The tumor xenograft and fluorescence imaging were confirmed the tumor growth *in vivo*. In summary, overexpression of miR-200c-3p inhibited cell proliferation and invasion of nephroblastoma cell , which were consistent with the results reported in other cancer cells [30, 31], suggesting that miR-200c-3p plays an anti-proliferating role in the progression of nephroblastoma. The analysis of bioinformatica databased showed that EP300 maybe a target gene of miR-200c-3p. From the results of mRNA target-predicting algorithms, we proposed that miR-200c-3p might be a novel negative regulator for EP300. Moreover, luciferase activity assay confirmed that miR-200c-3p directly targeted the 3'UTR of EP300. Western blot showed that the expression of miR-200c-3p was negative correlated with target gene EP300. Previous studies suggested that EP300 may be involved in oncogenic

11

349 processes in several different carcinomas including lung, prostate, laryngeal squamous cell cancer,

350 breast cancer and leukemia [32-36]. These results suggested that miR-200c-3p played an anti-

351 tumour role targeting EP300 in nephroblastoma. In addition, in this study, luciferase activity assay

352 confirmed that CCNE2 was also the target gene of miR-200c-3p. Cyclin E2 (CCNE2) has been

353 identified as the second member of E-type CDKs, which contributes to the G1/S phase transition,

354 cell proliferation, tumorigenesis and cancer progression. However, EP300 regulates transcription by

355 serving as scaffolds that bridge sequence-specific DNA binding factors and the basal transcriptional

356 machinery, thereby facilitating transcription through acetylation of histones, transcription factors,

357 and autoacetylation. Finally, EP300 was selected as the research object to explore its signal

358 transduction pathway.

359 It is also well established that EP300 is able to interact with AKT and play a key role in accelerating

360 cancer invasion and metastasis [37]. The AKT/FOXO1 signaling pathway paly a key role s in

361 modulating tumor cell proliferation, inhibition of cell cycle, survival and apoptosis in several cancer

362 types [38-41]. We hypothesized that miR-200c-3p might participate in the proliferation and

363 invasion of nephroblastoma by inhibiting the AKT/FOXO1 signaling pathway. FOXO1, a

364 transcription factor that is negatively regulated by AKT-mediated phosphorylation, has been

365 considered to regulate the expression of many genes that are crucial for cell proliferation and

366 invasion. Cyclin dependent kinase inhibitor p27 (also known as Kip1) can regulate the proteolytic

367 degradation and exclusion from the nucleus to inhibit the proliferation of cancers. In quiescent cells,

368 FOXO1 is located in the nucleus in which it can directly bind to the p27 promoter and activate its

369 transcription. In response to oncogenic signals, FOXO1 is phosphorylated by AKT, resulting in

370 nuclear export and retention in the cytoplasm leading to interference in p27 transcription function

371 and thus promoting cell proliferation [42]. Our results validated that miR-200c-3p can decrease the

372 AKT phosphorylation and activation, and leading to high expression and transcriptional activity of

373 FOXO1, which further upregulated the expression of p27. Notably, this study revealed that the

374 transcription factor P27 could bind into the EP300 promoter. In addition, a previous study has

375 demonstrated that the interaction between AKT and EP300 can maintain a steady state level of

376 EP300 and enter the G1 phase of the cell cycle [43]. These results suggested miR-200c-3p can

377 decrease the expression of EP300, and then regulate AKT/FOXO1/p27 signaling pathway to

378 participate in nephroblastoma proliferation and invasion.

379 In summary, our study showed that miR-200c-3p was downregulated in nephroblastoma tissues and

380 cells and played a key role in the progression of nephroblastoma. Moreover, we found that miR-

381 200c-3p inhibits the proliferation and invasion of nephroblastoma by targeting EP300 and

382 inactivating AKT/FOXO1/p27 pathway. The molecular mechanisms explored in this study may

383 provide new insights and therapeutic strategies for nephroblastoma prevention and treatment.

384

387

388 **Supplementary data are available in the online version of the paper.**

389

390

391 **References**

392 [1] JIA W, DENG Z, ZHU J, FU W, ZHU S et al. Association Between HACE1 Gene
393   Polymorphisms and Wilms' Tumor Risk in a Chinese Population. Cancer Invest 2017; 35:
394   633-638. https://doi.org/10.1080/07357907.2017.1405016

395 [2] LOPYAN NM, EHRLICH PF. Surgical Management of Wilms Tumor (Nephroblastoma)
396   and Renal Cell Carcinoma in Children and Young Adults. Surg Oncol Clin N Am 2021; 30:
397   305-323. https://doi.org/10.1016/j.soc.2020.11.002

398 [3] VUJANIC GM, GESSLER M, OOMS AHAG, COLLINI P, COULOMB-HERMINE A et
399   al. The UMBRELLA SIOP-RTSG 2016 Wilms tumour pathology and molecular biology
400   protocol. Nat Rev Urol 2018; 15: 693-701. https://doi.org/10.1038/s41585-018-0100-3

401 [4] GADD S, HUFF V, WALZ AL, OOMS AHAG, ARMSTRONG AE et al. A Children's
402   Oncology Group and TARGET initiative exploring the genetic landscape of Wilms tumor.
403   Nat Genet 2017; 49:1487-1494. https://doi.org/10.1038/ng.3940

404 [5] ZHAO XS, TAO N, ZHANG C, GONG CM, DONG CY. Long noncoding RNA MIAT acts
405   as an oncogene in Wilms' tumor through regulation of DGCR8. Eur Rev Med Pharmacol Sci
406   2019; 23: 10257-10263. https://doi.org/10.26355/eurrev_201912_19663

407 [6] PALCULICT TB, RUTESHOUSER EC, FAN Y, WANG W, STRONG L et al.
408   Identification of germline DICER1 mutations and loss of heterozygosity in familial Wilms
409   tumour. J Med Genet 2016; 53: 385-388. https://doi.org/10.1136/jmedgenet-2015-103311

410 [7] KALISH JM, DOROS L, HELMAN LJ, HENNEKAM RC, KUIPER RP et al. Surveillance
411   Recommendations for Children with Overgrowth Syndromes and Predisposition to Wilms
412   Tumors and Hepatoblastoma. Clin Cancer Res 2017; 23: e115-e122.
413   https://doi.org/10.1158/1078-0432.CCR-17-0710

414 [8] STAVAST CJ, ERKELAND SJ. The Non-Canonical Aspects of MicroRNAs: Many Roads
415   to Gene Regulation. Cells 2019; 8: 1465-1478. https://doi.org/10.3390/cells8111465

416 [9] XIAO M, LI J, LI W, WANG Y, WU F et al. MicroRNAs activate gene transcription
417   epigenetically as an enhancer trigger. RNA Biol 2017; 14: 1326-1334.
418   https://doi.org/10.1080/15476286. 2015.1112487

13

419 [10] ABDI A, ZAFARPIRAN M, FARSANI ZS. The Computational Analysis Conducted on
420   miRNA Target Sites in Association with SNPs at 3'UTR of ADHD-implicated Genes. Cent
421   Nerv   Syst   Agents   Med   Chem   2020;   20:   58-75.
422   https://doi.org/10.2174/1871524919666191014104843

423 [11] SCHUSTER SL, HSIEH AC. The Untranslated Regions of mRNAs in Cancer. Trends
424   Cancer 2019; 5: 245-262. https://doi.org/10.1016/j.trecan.2019.02.011

425 [12] KHAN AQ, AHMED EI, ELAREER NR, JUNEJO K, STEINHOFF M et al. Role of
426   miRNA-Regulated Cancer Stem Cells in the Pathogenesis of Human Malignancies. Cells
427   2019; 8: 840-854. https://doi.org/10.3390/cells8080840

428 [13] WANG C, ZHOU H, XUE Y, LIANG J, NARITA Y et al. Epstein-Barr Virus Nuclear
429   Antigen Leader Protein Coactivates EP300. J Virol 2018; 92: 2155-2173. https://doi.org/10.
430   1128/JVI.02155-17

431 [14] DU Y, CHI X, AN W. Downregulation of microRNA-200c-3p reduces damage of
432   hippocampal neurons in epileptic rats by upregulating expression of RECK and inactivating
433   the   AKT   signaling   pathway.   Chem   Biol   Interact   2019;   307:   223-233.
434   https://doi.org/10.1016/j.cbi.2019.04.027

435 [15] YANG Y, FANG T, CAO YL, LV YX, CHANG QQ et al. Ethyl Acetate Fraction from
436   Hedyotis diffusa plus Scutellaria barbata Exerts Anti-Breast Cancer Effect via miR-200c-
437   PDE7B/PD-L1-AKT/MAPK Axis. Evid Based Complement Alternat Med 2020; 2020: 1-
438   14. https://doi.org/10.1155/2020/3587095

439 [16] XUAN W, YU H, ZHANG X, SONG D. Crosstalk between the lncRNA UCA1 and
440   microRNAs in cancer. FEBS Lett 2019; 593: 1901-1914. https://doi.org/10.1002/1873-
441   3468.13470

442 [17] WANG H, CAI X, MA L. Curcumin Modifies Epithelial-Mesenchymal Transition in
443   Colorectal Cancer Through Regulation of miR-200c/EPM5. Cancer Manag Res 2020; 12:
444   9405-9415. https://doi: 10.2147/CMAR.S260129

445 [18] MEI J, WANG DH, WANG LL, CHEN Q, PAN LL, et al. MicroRNA-200c suppressed
446   cervical cancer cell metastasis and growth via targeting MAP4K4. Eur Rev Med Pharmacol
447   Sci 2018; 22: 623-631. https:/doi: 10.26355/eurrev_201802_14286

448 [19] LIU J, WANG L, LI X. HMGB3 promotes the proliferation and metastasis of glioblastoma
449   and is negatively regulated by miR-200b-3p and miR-200c-3p. Cell Biochem Funct 2018;
450   36: 357-365. https:/doi: 10.1002/cbf.3355

451 [20] ANASTASIADOU E, MESSINA E, SANAVIA T, MUNDO L, FARINELLA F et al. MiR-
452   200c-3p contrasts PD-L1 induction by combinatorial therapies and slows proliferation of
453   epithelial ovarian cancer through Downregulation of β-Catenin and c-Myc. Cells 2021; 10:
454   519-540. https:/doi: 10.3390/cells10030519

455 [21] LI S, FENG Z, ZHANG X, LAN D, WU Y. Up-regulation of microRNA-200c-3p inhibits
456   invasion and migration of renal cell carcinoma cells via the SOX2-dependent Wnt/β-catenin
457   signaling pathway. Cancer Cell Int 2019; 19: 231-244. https://doi: 10.1186/s12935-019-
458   0944-5

459 [22] IWASAKI H, ICHIHARA Y, MORINO K, LEMECHA M, SUGAWARA L et al.
460   MicroRNA-494-3p inhibits formation of fast oxidative muscle fibres by targeting E1A-
461   binding protein p300 in human-induced pluripotent stem cells. Sci Rep 2021; 11: 1161-
462   1175. https://doi.org/10.1038/ s41598-020-80742-y

463 [23] ROPOLO A, CATRINACIO C, RENNA FJ, BOGGIO V, ORQUERA T et al. A Novel
464   E2F1-EP300-VMP1 Pathway Mediates Gemcitabine-Induced Autophagy iRINOn
14

465 Pancreatic Cancer Cells Carrying Oncogenic KRAS. Front Endocrinol (Lausanne) 2020; 11:
466 411-425. https://doi.org/10.3389/fendo.2020.00411

467 [24] RING A, KAUR P, LANG JE. EP300 knockdown reduces cancer stem cell phenotype,
468 tumor growth and metastasis in triple negative breast cancer. BMC Cancer 2020; 20: 1076-
469 1090. https://doi: 10.1186/s12885-020-07573-y

470 [25] HUANG YH, CAI K, XU PP, WANG L, HUANG CX et al. CREBBP/EP300 mutations
471 promoted tumor progression in diffuse large B-cell lymphoma through altering tumor-
472 associated macrophage polarization via FBXW7-NOTCH-CCL2/CSF1 axis. Signal
473 Transduct Target Ther 2021; 6: 10-24. https://doi: 10.1038/s41392-020-00437-8

474 [26] BI Y, KONG P, ZHANG L, CUI H, XU X et al. EP300 as an oncogene correlates with poor
475 prognosis in esophageal squamous carcinoma. J Cancer 2019; 10: 5413-5426. https:/doi:
476 10.7150/jca.34261

477 [27] WANG D, CUI Y, XU A, ZHAN L, LI P. MiR-596 activated by EP300 controls the
478 tumorigenesis in epithelial ovarian cancer by declining BRD4 and KPNA4. Cancer Cell Int
479 2020; 20: 447-460. https://doi.org/10.1186/s12935-020-01497-0

480 [28] GARCIA-CARPIZO V, RUIZ-LLORENTE S, SARMENTERO J, GONZALEZ-CORPAS
481 A, BARRERO MJ. CREBBP/EP300 Bromodomain Inhibition Affects the Proliferation of
482 AR-Positive Breast Cancer Cell Lines. Mol Cancer Res 2019; 17: 720-730.
483 https://doi.org/10.1158/1541-7786.MCR-18-0719

484 [29] ATTAR N, KURDISTANI SK. Exploitation of EP300 and CREBBP Lysine
485 Acetyltransferases by Cancer. Cold Spring Harb Perspect Med 2017; 7: 1-15. https:/doi:
486 10.1101/cshperspect. a026534

487 [30] MAOLAKUERBAN N, AZHATI B, TUSONG H, ABULA A, YASHENG A et al. MiR-
488 200c-3p inhibits cell migration and invasion of clear cell renal cell carcinoma via regulating
489 SLC6A1. Cancer Biol Ther 2018; 19: 282-291.
490 https://doi.org/10.1080/15384047.2017.1394551

491 [31] LIU J, WANG L, LI X. HMGB3 promotes the proliferation and metastasis of glioblastoma
492 and is negatively regulated by miR-200b-3p and miR-200c-3p. Cell Biochem Funct 2018;
493 36: 357-365. https://doi.org/10.1002/cbf.3355

494 [32] KIM BR, COYAUD E, LAURENT EMN, ST-GERMAIN J, VAN DE LAAR E et al.
495 Identification of the SOX2 Interactome by BioID Reveals EP300 as a Mediator of SOX2-
496 dependent Squamous Differentiation and Lung Squamous Cell Carcinoma Growth. Mol Cell
497 Proteomics 2017; 16: 1864-1888. https://doi.org/10.1074/mcp.M116.064451

498 [33] ZOU LJ, XIANG QP, XUE XQ, ZHANG C, LI CC et al. Y08197 is a novel and selective
499 CBP/EP300 bromodomain inhibitor for the treatment of prostate cancer. Acta Pharmacol Sin
500 2019; 40: 1436-1447. https://doi.org/10.1038/s41401-019-0237-5

501 [34] DOGAN S, XU B, MIDDHA S, VANDERBILT CM, BOWMAN AS et al. Identification of
502 prognostic molecular biomarkers in 157 HPV-positive and HPV-negative squamous cell
503 carcinomas of the oropharynx. Int J Cancer 2019; 145: 3152-3162.
504 https://doi.org/10.1002/ijc.32412

505 [35] RING A, KAUR P, LANG JE. EP300 knockdown reduces cancer stem cell phenotype,
506 tumor growth and metastasis in triple negative breast cancer. BMC Cancer 2020; 20: 1076-
507 1090. https://doi.org/10.1186/s12885-020-07573-y

508 [36] JING Y, LI YF, WAN H, LIU DH. Detection of EP300-ZNF384 fusion in patients with
509 acute lymphoblastic leukemia using RNA fusion gene panel sequencing. Ann Hematol
510 2020; 99: 2611-2617.https://doi.org/10.1007/s00277-020-04251-8

15

[37] LI G, YANG Q, YANG Y, YANG G, WAN J et al. Laminar shear stress alters endothelial KCa2.3 expression in H9c2 cells partially via regulating the PI3K/Akt/p300 axis. Int J Mol Med 2019; 43: 1289-1298. https://doi.org/10.3892/ijmm.2019.4063

[38] WU Z, QIU M, MI Z, MENG M, GUO Y et al. WT1-interacting protein inhibits cell proliferation and tumorigenicity in non-small-cell lung cancer via the AKT/FOXO1 axis. Mol Oncol 2019; 13: 1059-1074. https://doi.org/10.1002/1878-0261.12462

[39] PAN S, DENG Y, FU J, ZHANG Y, ZHANG Z et al. Decreased expression of ARHGAP15 promotes the development of colorectal cancer through PTEN/AKT/FOXO1 axis. Cell Death Dis 2018; 9: 673-687. https://doi.org/10.1038/s41419-018-0707-6

[40] WU Z, NIU T, XIAO W. Uev1A promotes breast cancer cell survival and chemoresistance through the AKT-FOXO1-BIM pathway. Cancer Cell Int 2019; 19: 331-345. https://doi.org/10.1186/s12935-019-1050-4

[41] DENG JL, ZHANG R, ZENG Y, ZHU YS, WANG G. Statins induce cell apoptosis through a modulation of AKT/FOXO1 pathway in prostate cancer cells. Cancer Manag Res 2019; 11: 7231-7242. https://doi.org/10.2147/CMAR.S212643

[42] YANG F, CHEN E, YANG Y, HAN F, HAN S et al. The Akt/FoxO/p27Kip1 axis contributes to the anti-proliferation of pentoxifylline in hypertrophic scars. J Cell Mol Med 2019; 23: 6164-6172. https://doi.org/10.1111/jcmm.14498

[43] OGIWARA H, SASAKI M, MITACHI T, OIKE T, HIGUCHI S et al. Targeting p300 Addiction in CBP-Deficient Cancers Causes Synthetic Lethality by Apoptotic Cell Death due to Abrogation of MYC Expression. Cancer Discov 2016; 6: 430-445. https://doi.org/10.1158/2159-8290.CD-15-0754

Figure Legends

Figure 1. miR-200c-3p is downregulated in nephroblastoma tissues and cells. A) heat map of miRNAs expression array in the indicated nephroblastoma tissues (Tumor T1-3) and adjacent non-neoplastic renal tissues (N1-3, n=3/group). B, C) Real-time PCR performed for miR-200c-3p expression in 22 nephroblastoma tissues and corresponding non-neoplastic renal tissues . Data are represented as mean±SD. **$p < 0.01$ D) MiR-200c-3p expression in nephroblastoma cells. *$p < 0.05$

Figure 2. EP300 is a bona fide target of miR-200c-3p in nephroblastoma. A) Schematic diagram showing EP300-3'UTR. Sequences were compared between the miR-200c-3p and the wild-type (WT) or mutant (Mut) putative target sites in the 3'UTR of EP300 mRNA. B) Luciferase activities of wild-type 3'UTR EP300-luc and mutant 3'UTR EP300-luc constructs in G401 cells transfected with miR-200c-3p plasmid. Data are represented as mean±SD. *$p < 0.05$ C) Western blot analysis showing EP300 expression in SK-NEP-1 and G401 cells transfected with miR-200c-3p mimic or

549 miR-200c-3p inhibitor.   ***p < 0.001

550

551 **Figure 3.** miR-200c-3p suppresses tumor proliferation in nephroblastoma. A) Effect of miR-200c-

552 3p mimic or inhibitor on proliferation of SK-NEP-1 and G401 cells demonstrated by CCK8 assay.

553 Data are represented as mean±SD. *p < 0.05, **p < 0.01 B) Effects of miR-200c-3p mimic or

554 inhibitor on cell proliferation in G401 cells by colony formation assay. Data are represented as

555 mean±SD. *p < 0.05

556

557 Figure 4. miR-200c-3p suppresses tumor proliferation in nephroblastoma. A) Effects of miR-200c-

558 3p mimic or inhibitor on cell proliferation in SK-NEP-1 and G401 cells by soft agar assay. Data are

559 represented as mean±SD. *p < 0.05. B) Effects of miR-200c-3p mimic or inhibitor on cell cycle in

560 SK-NEP-1 and G401 cells. Data are represented as mean±SD. *p < 0.05

561

562 **Figure 5.** miR-200c-3p suppresses invasion and migration of nephroblastoma cells. A) Effect of

563 miR-200c-3p mimic or inhibitor on the invasion of G401 cells, as tested by transwell assay.

564 Morphologic comparison of cells penetrating the artificial basement membrane is shown. Data are

565 represented as mean±SD. *p < 0.05. B) Effects of miR-200c-3p mimic or inhibitor on cell

566 migration of G401 cells demonstrated using wound healing assay. Data are represented as

567 mean±SD. *p < 0.05

568

569 **Figure 6.** miR-200c-3p suppresses tumor grouth of nephroblastoma. Subcutaneous tumors of nude

570 mice injected with miR-200c-3p mimic or inhibitor. A) The pathological changes of mice with

571 different groups by Hematoxylin-eosin (HE) staining. B) The nodular volume of subcutaneous

572 tumors are shown. Data are represented as mean±SD. *p < 0.05 C) The tumor formation of nude

573 mice with different groups at 14 and 28 days after transplantation by *in vivo* fluorescence imaging.

574

575 **Figure 7.** miR-200c-3p is involved in AKT/FOXO1/p27 signaling pathways in nephroblastoma. A)

576 Western blot analyses of AKT, p-Akt, FOXO1, p-FOXO1 and p27 in the cells as indicated. B) The

577 relationship between EP300 and P27 by chromatin immunoprecipitation assay. Data are represented

578 as mean±SD. *p < 0.05

579

580   **Table 1.** Primers designed according to the 3 binding site between EP300 promoter and P27 for
581   chromatin immunoprecipitation assay.

Gene	F/R	Primer Sequence	Product
p27KIP site1	F	ACAGGCCACATCAAGGAAAC	206
	R	CCGGAGTCAGGACTAGATGC	
p27KIP site2	F	ATGGCCTTAACTGTGCTTGG	206
	R	AGGAGTAGACGCGGCACTTA	
p27KIP site3	F	GCCATATTGGGCCACTAAAA	245
	R	AGTCTCCGCTGATCAAATGG	
GAPDH	F	GCCCATGTTGGTCTCAAACT	209
GAPDH	R	TGCCAACTGTCTCTGTCCAC	

582
583

584 **Table 2.** The mRNA levels of 9 candidate target genes of miR-200c-3p, including *AKT2*, *CRKL*,
585 *CBL*, *EP300*, *LAMC1*, *PTEN*, *E2F3*, *CCNE2*, and *CDK2*, in G401 cells, SK-NEP-1 cells and 293FT
586 cells.

Genes	293T (mean±SD)	G401 (mean±SD)	SK-NEP-1 (mean±SD)	F-value	p-value
AKT2	1.000±0.023	1.489±0.067	1.810±0.038	93.93	< 0.001**
CRKL	1.000±0.018	0.377±0.018	0.121±0.002	1685.485	< 0.001**
CBL	1.000±0.051	1.306±0.096	1.577±0.036	26.145	0.001**
EP300	1.000±0.013	0.543±0.012	0.402±0.014	1294.406	< 0.001**
LAMC1	1.000±0.003	1.323±0.030	1.705±0.013	5945.717	< 0.001**
PTEN	1.000±0.009	0.180±0.031	0.112±0.005	1008.505	< 0.001**
E2F3	1.000±0.075	1.366±0.221	0.511±0.027	7.47	0.024*
CCNE2	1.000±0.037	0.051±0.010	0.320±0.007	648.155	< 0.001**
CDK2	1.000±0.036	0.238±0.010	0.295±0.001	611.162	< 0.001**

587 *p < 0.05, **p < 0.001

588

589 **Table 3.** The mRNA levels of 9 candidate target genes of miR-200c-3p, including *AKT2*, *CRKL*,
590 *CBL*, *EP300*, *LAMC1*, *PTEN*, *E2F3*, *CCNE2*, and *CDK2*, in G401 cells transfected with miR-200c-
591 3p mimic and mimic NC.

Genes	Mimic NC	miRNA-200c mimic	F-value	p-value
AKT2	1.000±0.075	0.030±0.001	3.978	0.004*
CRKL	1.000±0.030	0.356±0.015	0.016	0.000**
CBL	1.000±0.016	0.427±0.011	0.03	0.000**
EP300	1.000±0.037	0.460±0.035	0.351	0.001**
CCNE2	1.000±0.051	0.342±0.032	0.013	0.001**
PTEN	1.000±0.056	0.957±0.031	0.53	0.645
E2F3	1.000±0.057	0.804±0.013	0.003	0.019*
LAMC1	1.000±0.027	1.006±0.053	3.039	0.000**
CDK2	1.000±0.025	0.785±0.038	3.276	0.000**

592 *p < 0.05, **p < 0.001

Fig. 2

A

EP300 3'UTR ———————————————■————————————— (12-17bp)

WT-EP300 5'... gaCATACACTAGAGACACCTTGT**AGTATT**t...3'
                                    | | | | | |
miR-200c-3P 3'... agGUA-GUAA----------UGGGCCGUCAUAAu 5'

MUT-EP300 5'... gaCATACACTAGAGACACCTTGT**AGCTCC**t...3'

B

EP300

■ mimic NC
□ miR-200c-3p mimics

WT: *
MUT: ns

C

SK-NEP-1 / G-401

EP300, GAPDH (SK-NEP-1)
EP300, GAPDH (G-401)

Lanes: Blank, mimic NC, miR-200c-3p mimic, inhibitor NC, miR-200c-3p inhibitor

■ Blank
□ mimic NC
■ miR-200c-3p mimic
□ inhibitor NC
■ miR-200c-3p inhibitor

SK-NEP-1: ***
G-401: ***
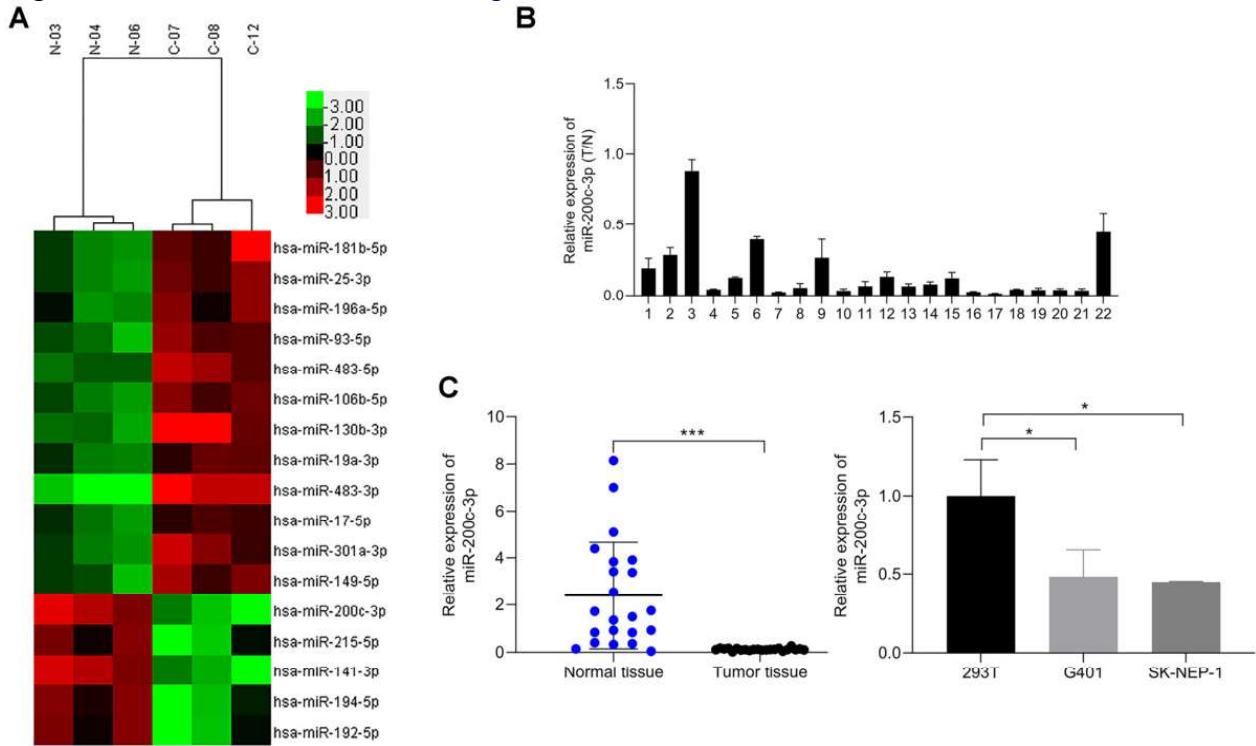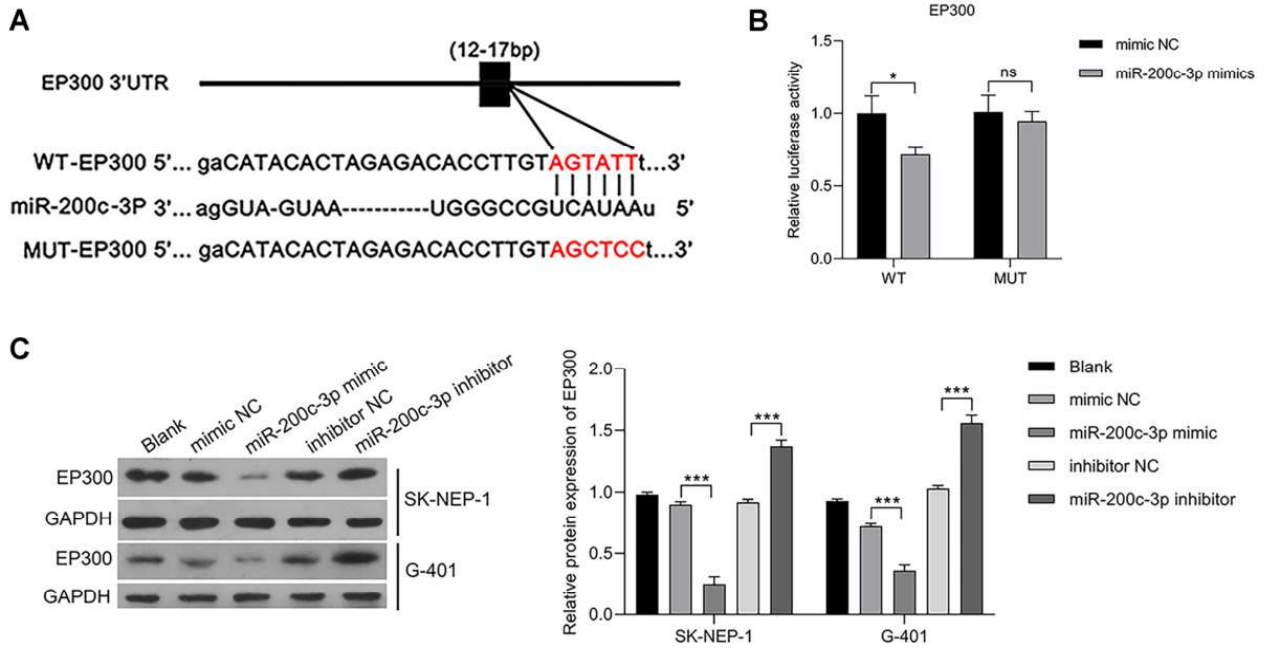
Fig. 3   <u>Download full resolution image</u>
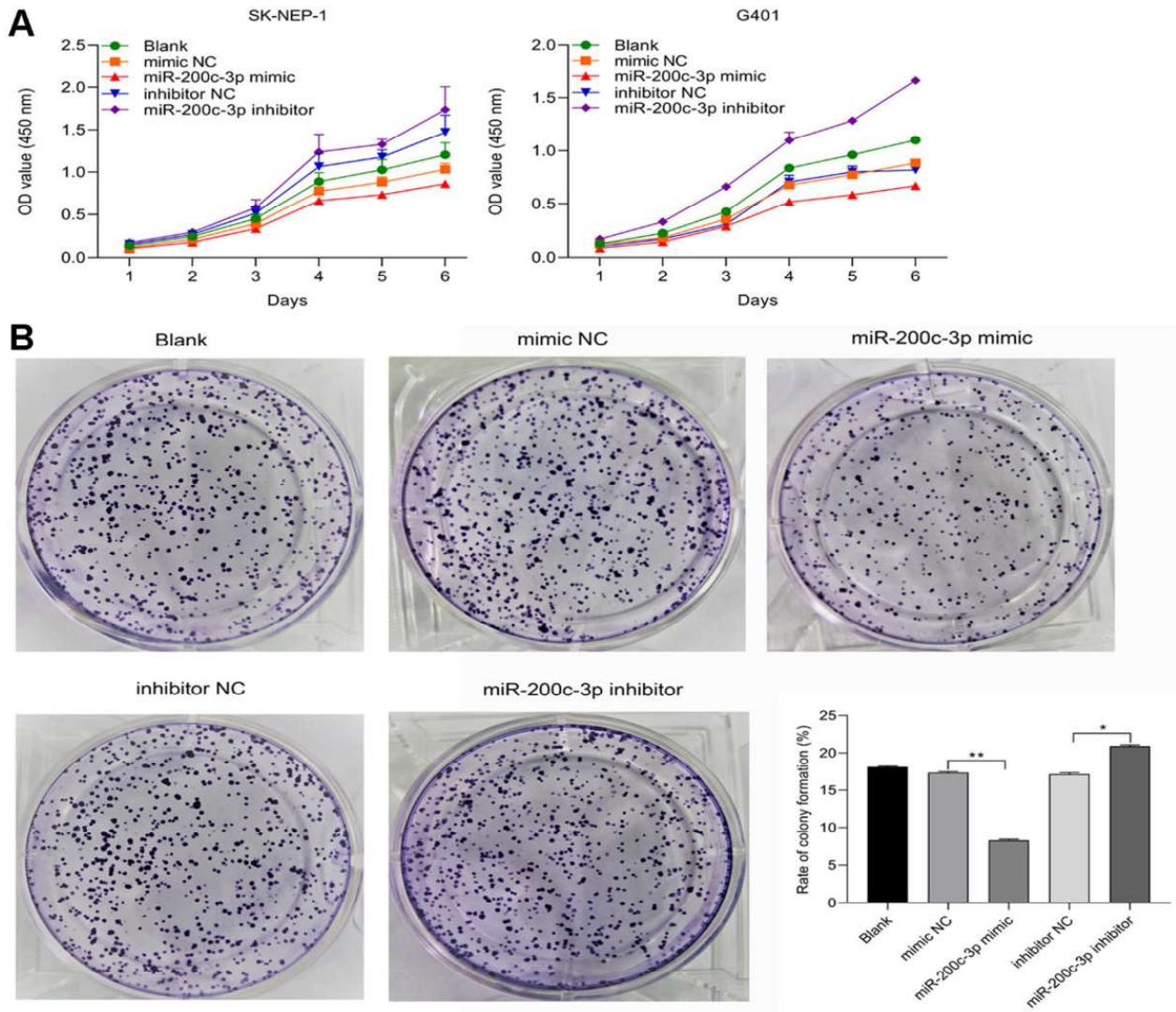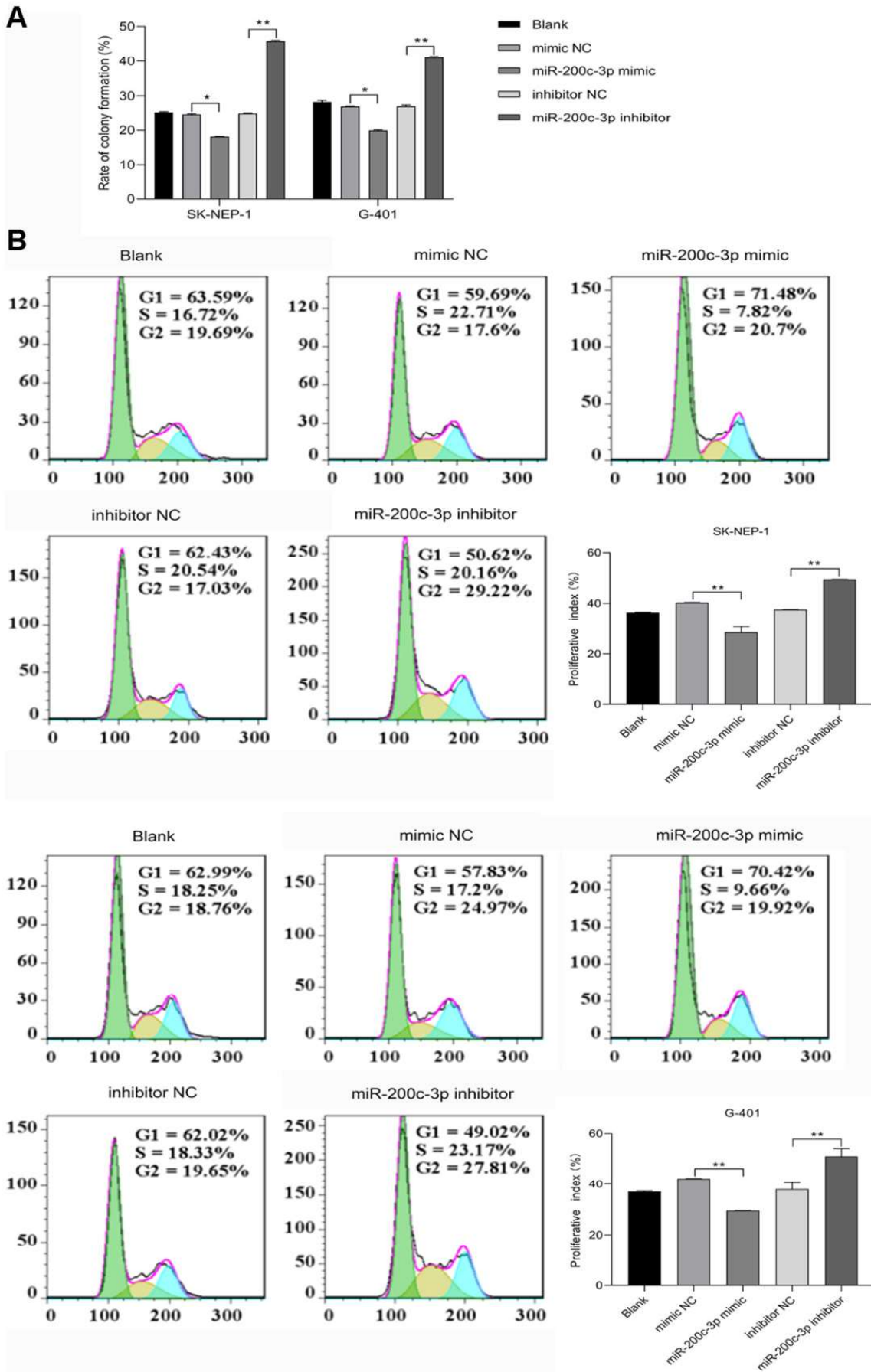
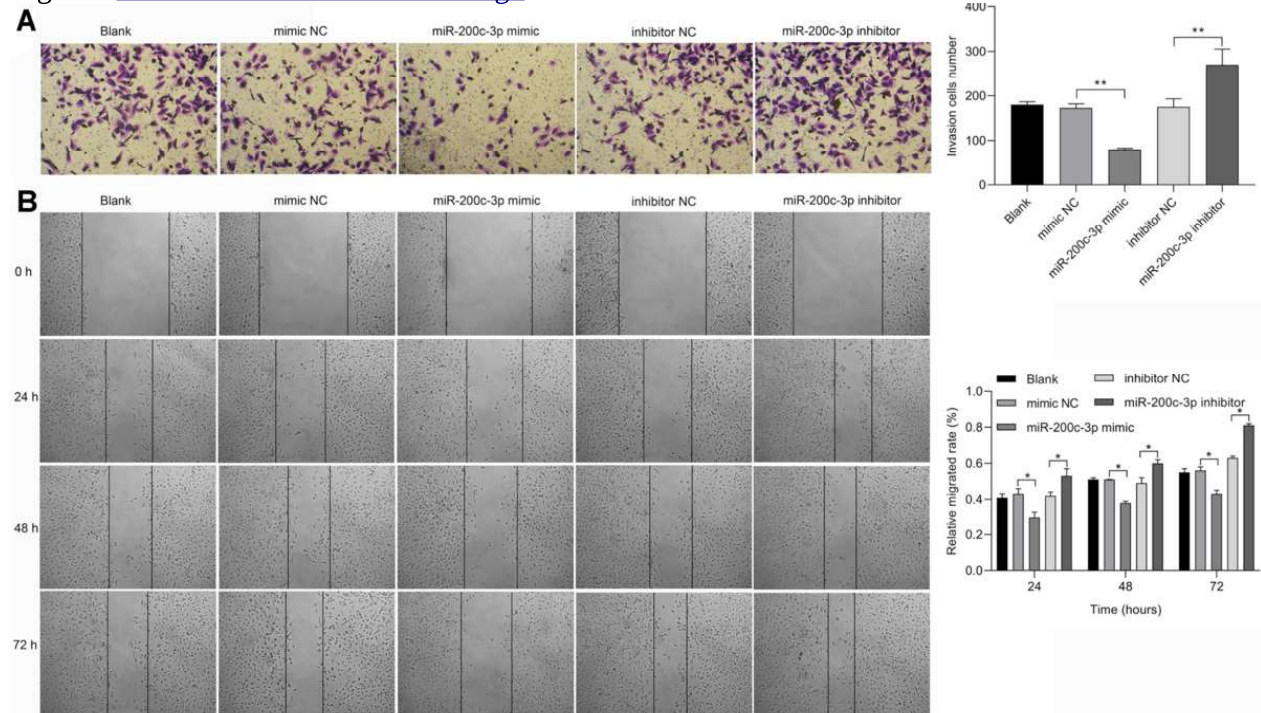Fig. 4   Download full resolution image

Fig. 5   [Download full resolution image](#)

Fig. 6   [Download full resolution image](#)

A

Blank   Mock   miR-200c-3p mimic   miR-200c-3p inhibitor

B

Blank   Mock   miR-200c-3p mimic   miR-200c-3p inhibitor
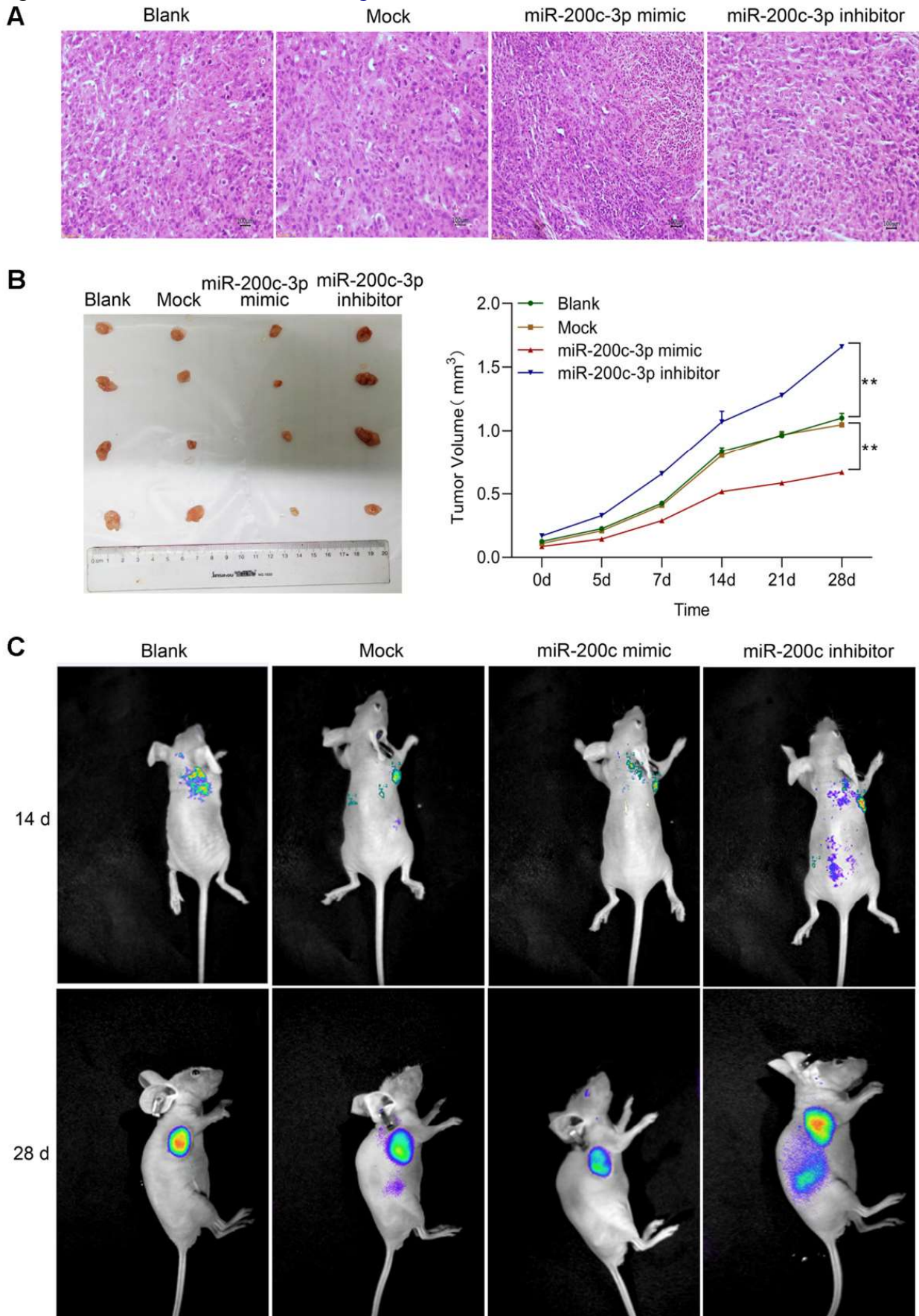
C

Blank   Mock   miR-200c mimic   miR-200c inhibitor

14 d

28 d

Fig. 7 [Download full resolution image](#)